Geologos 20, 2 (2014): 105–123
doi: 10.2478/logos-2014-0006

GEOLOGOS

Palaeo-earthquake events during the late Early Palaeozoic in the central Tarim Basin (NW China): evidence from deep drilling cores

Bizhu He[1,*], Xiufu Qiao[1], Cunli Jiao[2], Zhiqin Xu[1], Zhihui Cai[1], Xianpu Guo[1], Yinli Zhang[3]

[1] State Key Laboratory of Continental Dynamics and Tectonics, Institute of Geology, Chinese Academy of Geological Sciences, Beijing, China
[2] Exploration and Production Research Institute of SINOPEC, Beijing, China
[3] Institute of Mineral Resources; Chinese Academy of Geological Sciences, Beijing, China
* corresponding author; e-mail: hebizhu@vip.sina.com, hebizhu@cags.ac.cn

Abstract

Various millimetre-, centimetre- and metre-scale soft-sediment deformation structures (SSDS) have been identified in the Upper Ordovician and Lower-Middle Silurian from deep drilling cores in the Tarim Basin (NW China). These structures include liquefied-sand veins, liquefaction-induced breccias, boudinage-like structures, load and diapir- or flame-like structures, dish and mixed-layer structures, hydroplastic convolutions and seismic unconformities. The deformed layers are intercalated by undeformed layers of varying thicknesses that are petrologically and sedimentologically similar to the deformed layers.

The SSDS developed in a shelf environment during the early Late Ordovician and formed initially under shear tensile stress conditions, as indicated by boudinage-like structures; during the latest Ordovician, SSDS formed under a compressional regime. The SSDS in the Lower-Middle Silurian consist mainly of mixed layers and sand veins; they formed in shoreline and tidal-flat settings with liquefaction features indicating an origin under a compressional stress regime. By Silurian times, the centre of tectonic activity had shifted to the south-eastern part of the basin.

The SSDS occur at different depths in wells that are close to the syn-sedimentary Tazhong 1 Fault (TZ1F) and associated reversed-thrust secondary faults. Based on their characteristics, the inferred formation mechanism and the spatial association with faults, the SSDS are interpreted as seismites. The Tazhong 1 fault was a seismogenic fault during the later Ordovician, whereas the reversed-direction secondary faults became active in the Early-Middle Silurian.

Multiple palaeo-earthquake records reflect pulses and cyclicity, which supports secondary tectonic activity within the main tectonic movement. The range of SSDS structures reflects different developments of tectonic activity with time for the various tectonic units of the centralbasin. The effects of the strong palaeo-earthquake activity coincide with uplift, fault activity and syn-tectonic sedimentation in the study area during the Late Ordovician to Middle Silurian.

Keywords: soft-sediment deformation structures, seismites, palaeo-seismicity, Late Ordovician, Silurian, Tazhong 1 Fault, Tarim Basin

1. Introduction

Soft-sediment deformation structures (SSDS) are deformations that originated in unconsolidated sediments (Maltman, 1984, 1994; Brodzikowski & Van Loon, 1987; Qiao et al., 1994; Owen et al., 2011). Such deformations usually occur rapidly, at or close to the surface, during or shortly after deposition, and before lithification has taken place. SSDS are widely distributed. They can occur in different

structural settings: e.g. passive continental margins, deep (trench) subduction zones and strike-slip tectonic transitions, and they can form in almost all sedimentary environments, preferably in shallow-marine, lagoonal, lacustrine and fluvial environments (Allen, 1982; Maltman, 1984; Qiao et al., 1994; Rodríguez-López et al., 2007; He et al., 2011; Waldron & Gagnon, 2011; Owen et al., 2011; Du, 2011; Sarkar et al., 2014, this issue).

SSDS comprise a variety of brittle and plastic deformation styles with different geometries. These include load structures, convolutions, water-escape structures, slumps and collapse structures (Sims, 1978; Mills, 1983; Van Loon & Brodzikowski, 1987; Qiao et al., 1994, 2006; Montenat et al., 2007). The most common deformation mechanisms that give rise to SSDS include intergranular shear, plastic or hydroplastic flow, liquefaction and fluidisation. The resulting structures depend on the combination of the deformation mechanisms and the properties of the soft sediments (Lowe, 1975; Maltman, 1987; Owen, 1987; Guiraud & Plaziat, 1993; Qiao et al., 1994; Van Loon, 2009; Owen & Moretti, 2011).The triggers for near-surface soft-sediment deformation are tectonicism, glacigenic, mass movement, collapse and some other physical and biological processes (Seilacher, 1969; Qiao et al., 1994; McCalpin, 1996; Montenat et al., 2007; Van Loon, 2009; Owen et al., 2011; Du, 2011).

Earthquakes are commonly triggers of SSDS, especially because they may induce liquefaction and fluidisation (Seilacher, 1969; Qiao et al., 1994; Montenat et al., 2007; Ettensohn et al., 2011; Owen & Moretti, 2011). The term 'seismites' was first proposed by Seilacher (1969) to describe fault-graded beds in the Monterey shale (Miocene) resulting from palaeoseismic activity. Later, the term became commonly used to describe a variety of post-depositional and syn-depositional structures in unconsolidated sediments produced by seismic shocks. This was unfortunate (Van Loon, 2014a), as the original proposal concerned a layer, not structures. Moreover, a seismic origin of a specific SSDS can be established only if it is known for sure that the layer has been deformed by seismic activity. Therefore it is a good development that the term 'seismite' is nowadays used preferably again for earthquake-induced deformed layers, following the original proposal.

The criteria to assign a seismic origin to SSDS features have been discussed by numerous authors, among whom Seilacher (1969, 1984), Van Loon & Brodzikowski (1987), Qiao et al. (1994), Obermeier (1996), McCalpin (1996), Montenat et al. (2007), Qiao & Li (2009), Ettensohn et al. (2011) and Owen & Moretti (2011). The commonly accepted criteria include: (1) deformation in laterally continuous, vertically recurring layers, separated by undeformed layers; (2) occurrence in marine, lacustrine or fluvial sediments; (3) similar lithologies and facies features as the under- and overlying undeformed beds; (4) deformation consistent with a known seismogenic trigger; (5) systematic lateral changes in deformation regarding frequency, size and/or intensity toward a likely epicentral area. Even these criteria should, however, be handled with care (Moretti & Van Loon, 2014).

The varied and complex styles of deformation structures that are genetically related to seismic events are compatible with seismic shocks triggered by high–magnitude earthquakes. Based on comparisons with similar SSDS formed in modern seismically affected deposits, it can be deduced that such SSDS are related to surface-wave magnitudes of Ms>6 (Sims, 1975; Blanc et al., 1998). The most commonly found seismically induced SSDS in the sedimentary record are liquefied veins (sand or micrite veins: see, for instance, Üner, 2014, this issue), hydroplastic convolutions (see, for instance, Valente et al., 2014, this issue), fault grading and syn-sedimentary faults (see, for instance, Van Loon, 2014b, this issue), and loadcasts and pseudonodules (Seilacher, 1969; Sims, 1975; Qiao et al., 1994, 2006; Du & Han, 2000; Montenat et al., 2007; Wei et al., 2007; Song & Liu, 2009; Perucca et al., 2014, this issue).

The various morphology and deformation styles of the SSDS resulted from different driving forces, sediment rheology, deformation mechanisms and timing of the deformation with respect to sedimentation (Obermeier, 1996; Moretti et al., 1999; Qiao et al., 2006; Owen & Moretti, 2011). These parameters thus can help us to understand the depositional history with respect to contemporaneous tectonics, earthquakes, tsunamis, storms or other extreme events, as the sedimentary and early-diagenetic history are recorded in the sediments as well as secondary tectonic events during the main tectonic movements. Reconstruction of the the palaeogeographical environment can also be achieved. SSDS have therefore recently attracted increasing attention, also in drilling cores.

Several types of SSDS have been identified in cores from deep drilling wells that penetrate Silurian to Ordovician strata in the central Tarim Basin of NW China. These deformation structures are mainly small, ranging in size from several millimetres to several centimetres, but larger SSDS with vertical sizes up to a few metres have also been found. The SSDS that are observed in the Tarim cores were commonly mistaken for worm traces, mud cracks

or storm deposits since they have abrupt contacts with the surrounding sedimentary rock (according to the geological well reports). These interpretations were, however, not always justified: we examined SSDS in cores from 10 wells and related them to the sedimentary facies, depositional environments, stratigraphic position and proximity to faults. This led us to the conclusion that some of these SSDS meet the criteria of SSDS triggered by earthquakes, thus suggesting that they form part of seismites. In particular we propose boudinage-like SSDS and boudinage-like breccias which originally consisted of alternating mud and sand laminae that underwent shear tensional stress, resulting in metre-scale lenticular deformation structures, to be seismically induced. The seismic activity can be related to the activity of an adjacent fault.

The Tazhong 1 fault and the associated secondary reverse thrust faults were probably seismically active during the Late Ordovician to Middle Silurian. Their records of palaeo-seismicity reflect not only tectonic activity, but also the strength and frequency of the structural movements in the different parts of the faults. These SSDS are an important record of middle-late Caledonian tectonic movement and important supplementary evidence of the episodic character of these movements.

The present study, which is based on cores from deep wells in the Tarim Basin, is intended to provide new evidence of the tectonic activity, as well as clues that may increase the insight into the then environment, and into the properties and activity of the various faults in different time-spans. The study is also aimed at reducing the confusing interpretations of SSDS in cores. The more cores from wells are systematically and accurately analysed, the more the tectonics involved can be understood and correctly interpreted.

2. Geological setting

The Tarim Basin, located in north-western China, is the largest sedimentary basin (560,000 km^2) in that region. It is surrounded by the Tianshan Mountains in the north and west, the West Kunlun Mountains in the south-west and the Altun Mountains in the south-east (Fig. 1). The basin has undergone a long geological evolution with multiphase tectonic deformations from the Sinian (latest Neoproterozoic) to the Neogene. It is interpreted as a multicyclic or superimposed basin (He, 1995; Jia et al., 1995; Li et al., 1996; Tian & Zhang, 1997). The basin underwent three tectonic cycles, from the Sinian to the Middle Devonian, from the Late Devonian to

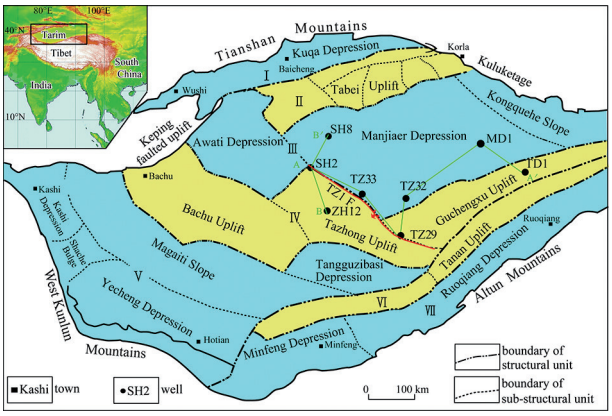

Fig. 1. Schematic map of the structural units of, and locations in the Tarim Basin.
Structural units: I = Kuqa Depression, II = Tabei Uplift Zone, III = Northern Depressions, IV = Central Uplift Zone, V = South-western Depression Zone, VI = Tanan Uplift Zone, VII = South-eastern Depression Zone.

the Permian, and from the Mesozoic to the Cenozoic respectively. It further experienced eight second-order tectonic events during, respectively, the early Caledonian, middle Caledonian, late Caledonian, Hercynian, Indosinian, Yanshanian, early Himalaya and Himalaya tectonic phases. Two unconformities, viz. Silurian/Upper Ordovician [= S/O_3] and Upper Devonian-Carboniferous/pre-Upper Devonian [= (D_3d+C)/An D_3d), (D_3d+C)/O_2, (D_3d+C)/O_3, (D_3d+C)/S)], were formed during the middle and late Caledonian tectonic movements (Jia et al., 1995; He, 1995; He et al., 2005, 2011, 2013; Jin et al., 2005; Tang & Jia, 2007).

The present study evaluates eight deep drilling wells in the Tazhong Uplift and the Manjiaer Depression in the central part of the basin. The Tazhong Uplift was a fault-controlled horst located in the middle part of the NW-SE trending central uplift zone. The main faults converge and become shallower to the south-east, whereas they spread and become deeper in the north-west. The Tazhong Uplift started to form during the Cambrian and Ordovician; it was uplifted further and became intensely folded, faulted, deformed and eroded during the Silurian to Late Devonian, and it basically became stable after Carboniferous deposition had stopped (He, 1995; Jia et al., 2004; Tang & Jia, 2007). The Manjiaer Depression is the largest sub-basin of the Tarim Basin (112,000 km^2) and contains the most complete stratigraphical succession within the Tarim Basin, comprising the Sinian to Neogene. The NW-SE striking Tazhong 1 fault (TZ1F) was the boundary fault between the Tazhong Uplift and the Manjiaer Depression during the Ordovician to Middle Devonian. Fault movement was strongest during the Ordovician, with a vertical fault displace-

ment in excess of 1 km. Fault displacement changed from initially normal faulting to reverse faulting during the late movements. Across the TZ1F fault, the stratigraphy changes drastically, with the Tazhong Uplift and the Manjiaer Depression being characterised by major thickness and lithological differences in the Middle to Late Ordovician (Jia et al., 2004; Zhao et al., 2010; He et al., 2009).

During the Ordovician, sedimentation in the Tarim Basin took place in a marine basin facies to shelf-and-platform depositional environment. The Tazhong Uplift and the Manjiaer Depression were located in this shelf-to-platform setting and the Ordovician succession is 600–3300 m thick. On the Tazhong Uplift (Table 1), the lower (O_1p and O_1y), the middle (O_2y) and upper Ordovician (O_3l) con-

Table 1. Stratigraphy of the Early Palaeozoic in the part of the Tarim Basin under study. The chronology follows Ogg et al. (2008). Stratigraphical subdivisions and correlations are modified after Zhao et al. (2000), Xu et al. (2005), Zhao et al. (2006) and Miao & Fu (2013).

Chronostratigraphy						Seismic reflection interface	Sequence Stratigraphy			Tectonic phase	Identified palaeo-earthquake events
Period	Epoch	Age	Age of boundary (Ma)	Tazhong Uplift	Manjiaer Depression		Sequence Boundary	Super sequence	Third-order sequence		
Devonian	Early	Emsian	407				Regional unconformity			Late Caledonian	
		Praghian	411	Keziertage Formation (S_3-D_2) k	Keziertage Formation (S_3-D_2) k						
		Lockhovian	416						SQ22		
Silurian	End-stage	Pridolian	419								
	Late	Ludfordian	421			T_6^1					
	Middle	Gorstian	423	Yimugantawu Formation S_2y	Yimugantawu Formation S_2y			SSQ3	SQ21		9
		Homerian	426			T_6^2					
	Early	Shenwooddian	428	Tataaiertage Formation S_1t	Tataaiertage Formation S_1t				SQ20		18
		Telychian	436			T_6^3					
		Aeronnian	439	Kepingtage Fm. S_1k	Kepingtage Formation (O_3-S_1) k				SQ19		2
		Rhuddanian	444	Absent Kepingtage Fm.		T_7^0	Regional unconformity		SQ18		
Ordovician	Late	Hirnantian	446						SQ14-17	Second stage of middle Caledonian	30
		Katian	447	Sangtamu Fm. O_3s	Queerqueke Formation O_3q			SSQ2			
			456	Lianglitage Fm. O_3l		T_7^2			SQ13		16
		Sandbian	461	Absent Qiaerbake Fm. O_3q		T_7^4	Local unconformity		SQ12		
	Middle	Darriwilian	468	Absent Yijianfang Fm. O_2y	Heituwa Formation O_2h	T_7^5		SSQ1	SQ11	First stage of Middle Caledonian	
		Dapingian	472								
	Early	Floian	479	Yinshan Formation O_1y	Tuershaketage Formation ($\in_3$-O_1) t	T_7^6			SQ10		
		Tremadocian	488	Penglaiba Fm. O_1p		T_8^0			SQ9		
Cambrain	Furongian	Furongian	499	Lower Qiulitage Gr. $\in_3q$		T_8^1			SQ8		

sist of carbonates, whereas the O_3s (uppermost formation of the Ordovician) consists of clastics. The O_2y is absent in the high part of the Tazhong Uplift, whereas the O_3q is entirely absent here.

During the Early to Middle Ordovician, the Manjiaer Depression was an undercompensation basin (i.e., a basin where sedimentation could not keep pace with subsidence) in which carbonaceous mudstone and siliceous radiolarians were deposited. This organic-rich O_2h unit is about 50–80 m thick.

During the Late Ordovician, the Manjiaer Depression was a flysch sub-basin The O_3q unit developed as a thick turbidite and terrigenous clastic shelf facies (Chen et al., 1999; Zhao et al., 2010). It consists predominantly of grey or dark grey mudstones and calcareous mudstones with intercalated siltstones, with a total thickness of up to 3000 m. The Tazhong Uplift and the transitional zone with the Manjiaer Depression developed into a rimmed carbonate platform during the Early to Middle Ordovician. The carbonate platform shrank to the central part of the Tazhong Uplift in response to the Late Ordovician transgression. During the early to middle Late Ordovician it had developed into an isolated platform/platform margin/slope system covering the present Tazhong Uplift and surrounding areas. During the middle Late Ordovician, the carbonate platform continued to shrink until it covered only the central part of the Tazhong Uplift. The O_3s unit represents the final drowning of the platform and is developed as a mixed shelf facies due to a transgression (Chen et al., 1999; Gu et al., 2005; Fan et al., 2007; He et al., 2009). The O_3s unit, which is about 700–1000 m thick, consists of dark grey to grey mudstones and calcareous mudstones and siltstones. An angular unconformity separates the Ordovician from the overlying Silurian in the Tazhong Uplift and in the southern part of the Manjiaer depression, with the largest stratigraphic gap south of the study area. Further to the north in the Manjiaer Depression, this angular unconformity changes into a disconformity.

During the Silurian to Middle Devonian, the Late Ordovician to Early Silurian Kepingtage Formation ($(O_3\text{-}S_1)k$), the Early Silurian Tataaiertage Formation (S_1t), the Middle Silurian Yimugantawu Formation (S_2y) and the Late Silurian to Middle Devonian Keziertage Formation ($(S_3\text{-}D_2)k$) were deposited across the Tazhong Uplift and the Manjiaer Depression. These offshore marine strata are up to 1700 m thick in the northern part of the Manjiaer Depression (Jia et al., 2004; He et al., 2011; Lin et al., 2011).

3. Description of the SSDS interpreted as seismically induced

In cores of eight, widely spaced (spacings > 100 km) exploration wells, we identified a variety of SSDS in the Upper Ordovician and Lower to Middle Silurian. They include veins of liquefied sand, liquefaction-induced breccias, mixed-layer structures, dish structures, ball-and-pillow structures, diapirs and flames, boudinage-like structures and convolutions (cf. Van Loon & Pisarska-Jamroży, 2014). Boudinage-like SSDS, which resulted from hydroplastic deformation and liquefaction, are common and reach metre-scale sizes in the cores of many wells in the study area.

3.1. Liquefied-sand veins

Sand veins are a vein-type structure that formed by injection of liquefied sand flow (Guiraud & Plaziat, 1993; Qiao et al., 1994; Obermeier, 1996; Qiao & Li, 2009). Unconsolidated near-surface sands that are water-saturated may liquefy when abruptly loaded or shaken. This results in overpressurising of the pore water, which may then escape to adjoining lower-pressure sites (i.e., commonly upwards) by forming injection features in otherwise undisturbed deposits (Nichols et al., 1994; Van Loon, 2009). Liquefied-sand injection veins are common in the studied cores and have been identified in wells MD1, TZ29, SH2 and Z12. They range in width from 2 mm to ~ 3 cm and their lengths range from 1 cm to over 10 cm.

At 5718.6 m depth in well MD1, thick horizontal mudstones interbedded with thin siltstones occur, which consist of unconsolidated shallow grey silty sand that became liquefied and intruded the greyish-black mud beds. These sand veins comprise two types, vertical (Fig. 2b, 1) and lateral (Fig. 2b, 2). The veins are irregularly curved, with occasional bifurcation in cross-section, and without a uniform planar direction in 3-D morphology. The textures and components of the sand veins are similar and differ clearly from the surrounding mudstones. The veins cut through mud beds and thus force arching or concave bending (Fig. 2a) of the surrounding laminated mud beds. Some of the sand veins are complex (Fig. 2c) and associated with liquefaction-induced breccias.

3.2. Liquefaction-induced breccias

Liquefaction-induced breccias are produced by liquefaction of sand that is both overlain and under-

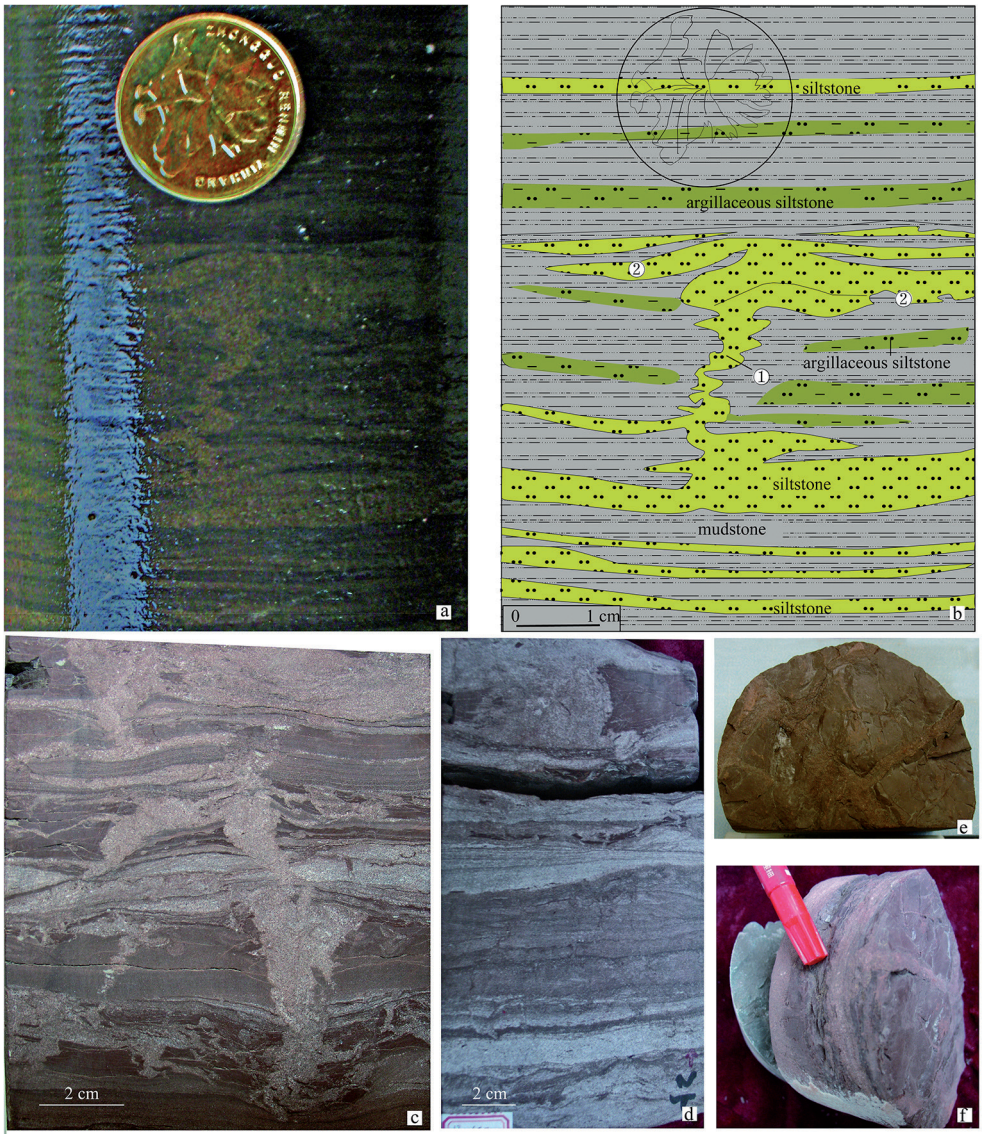

Fig. 2. Liquefied-sand veins in cores from wells in the Tarim Basin.
a: The width of the sand vein (below the coin) varies; the vein is twisted and the contact with the surrounding layers (dark grey mudstone intercalated with siltstone) is deformed by dragging. Well MD1, depth 5718.6 m; stratigraphical unit O_3q; **b**: Sketch of photo a. 1 = vertical sand veins, 2 = sill-like sand veins; **c:** Concentration of sand veins. Well SH2, depth 5567.3 m; stratigraphical unit S_2y; **d:** Wide (6 cm) sand vein (uppermost part of the core) connected with overlying liquefied host sand layer. Well SH2, depth 5573.2 m; stratigraphical unit S_2y; **e, f:** Sand veins in cross-section and plane, showing a plate-shaped morphology. Well SH2, depth 5573.1 m; stratigraphical unit S_2y.

lain by mud layers. Liquefaction of the sand caused disruption of the surrounding (semi)consolidated mud beds into gravel-sized, clayey breccia fragments. The breccias occur together with liquefied-sand veins (Fig. 3).

In well TZ29, at a depth of 5381 m (Fig. 3a, 3b), grey silty breccias are embedded in black grey mudstone; the breccias are composed of grey silty mudstone and siltstone fragments with angular and badly sorted particles of 0.3–1.5 cm. Similar breccias have been interpreted in the final well report as resulting from storm-induced currents. Our analysis shows, however, that the breccias were formed in the mud layers by injection of liquefied sand, ripping up and fragmenting the (semi)consolidated mud. Thus the breccias are in-situ and have not been transported. An interpretation as tempestites is consequently incorrect.

3.3. Diapirs/flames

Both diapirs and flames are plastic vertical or oblique intrusions that commonly end in some

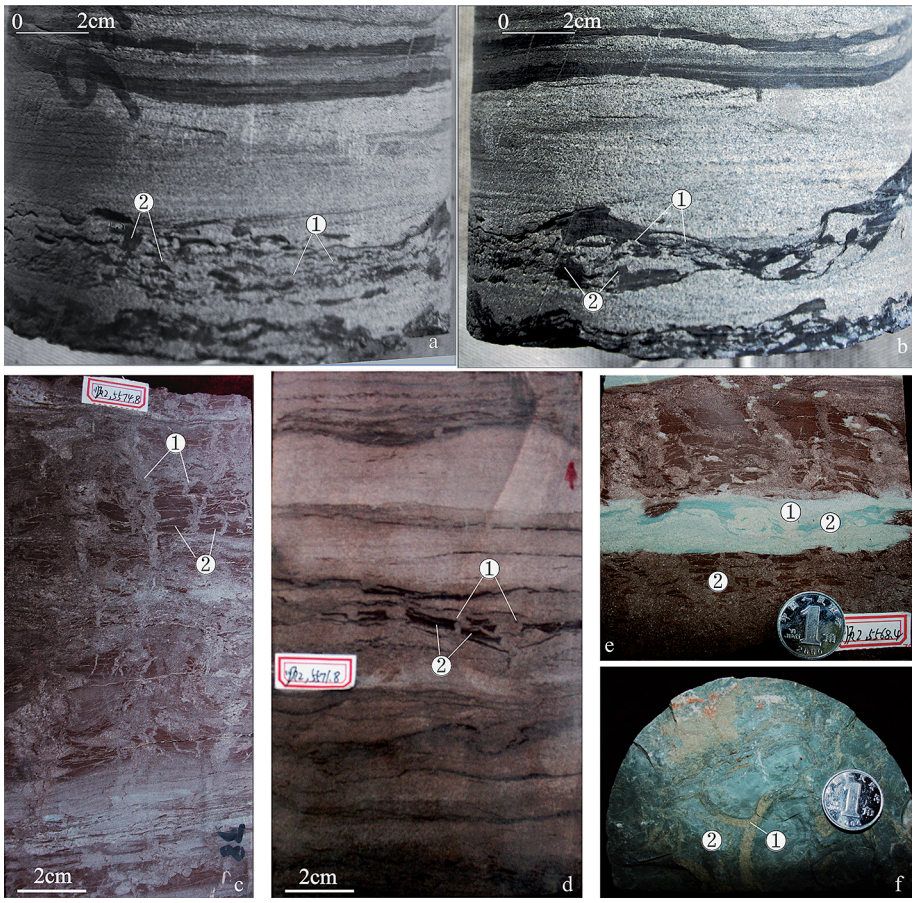

Fig. 3. Liquefaction-induced breccias in cores from the Tarim Basin. 1 = sand veins, 2 = liquefaction-induced breccias. **a, b:** Liquefaction-induced breccias formed due to lateral and vertical liquefaction of sands, with fragments showing an irregular and angular shape. The material consists of grey silty sands and strongly calcareous dark grey muds. Well TZ29, depth 5381.37 m; stratigraphical unit O_3s; **c:** Mainly vertical sand veins (4–6 mm wide, 2–3 cm long) injected into mud layers. Laterally extending sand veins broke off dark brown mud layers, resulting in liquefaction-induced breccias of dark brown mudstones. Well SH2, depth 5574.8 m; stratigraphical unit S_2y; **d:** Liquefaction-induced breccias in the central part of a core, showing fragments of dark brow mudstone. Well SH2, depth 5571.8 m; stratigraphical unit S_2y; **e, f:** Characteristics of liquefaction-induced breccias in cross-section (e) and on a bedding plane (f), previously misinterpreted as mud cracks. Well SH2, depth 5568.4 m; stratigraphical unit S_2y.

overlying bed that commonly becomes plastically deformed around the intruding material. Whether an SSDS should be called a diapir or a flame depends largely on its size. Small-scale centimetre- to decimetre-scale intrusions, as found commonly between adjacent loadcasts, tend to be called flames, whereas larger-scale SSDS are commonly called diapirs. Both are present in the cores under study. Common flames occur at a depth of 5381.3 m in well TZ29 in the Late Ordovician Sangtamu Fm. (Fig. 4a, 4b). The 3–5 cm thick grey calcareous silty sand layers are interbedded with 0.3–1 cm thick calcareous mud layers. During the deformation, the overlying calcareous silty sands sank downwards and the underlying calcareous mud intruded upwards but did not reach the sedimentary surface.

Liquefied diapirs/flames are commonly complex and have moved with a high energy in and upward direction after liquefaction. Often they follow an irregular 3-D pathway, so that they become visible at an exposed surface (or core) as 'xenoliths' (cf. Chen et al., 2009). The surrounding sediments are not only intruded, but also dragged, and they can become visible as intermittent layers or fragments (Qiao et al., 2006; Qiao & Li, 2009).

Such structures are identified in cores of well SH2 (Fig. 4c, 4d) at 5573.2 m depth. The close relationship between liquefied diapirs/flames and liquefied-sand veins is clearly visible.

3.4. Convolutions

The term ‘convolutions’ is used here to describe irregular folds with a wide variety in shape, scale, and properties of the axial plane. Convolutions

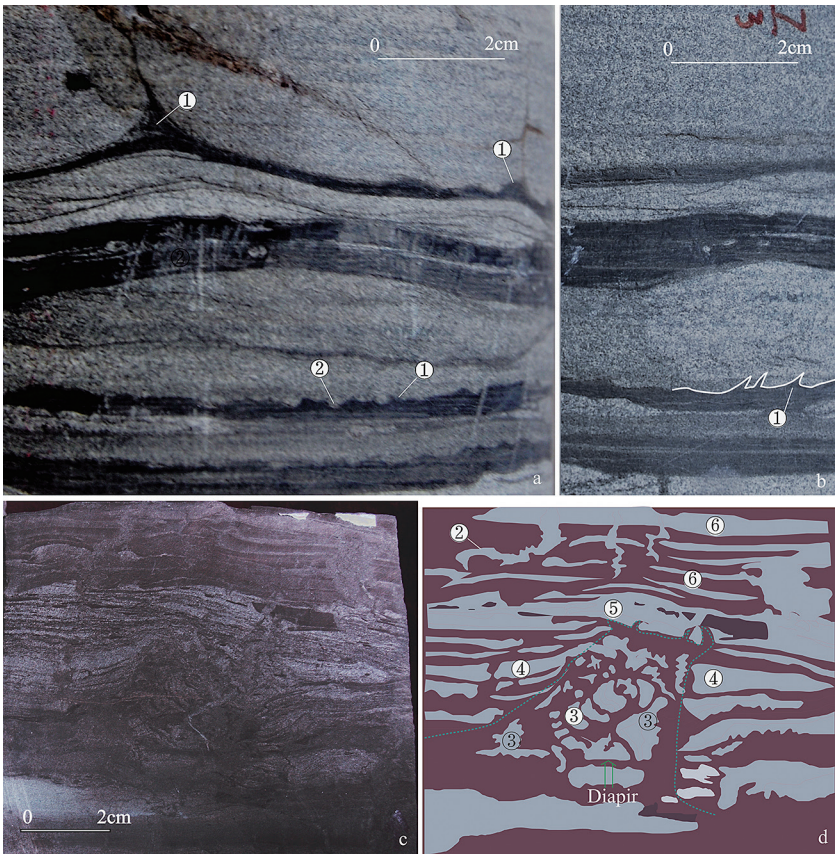

Fig. 4. Flame structures in cores from the Tarim Basin. 1 = diapir-like structures, 2 = liquefied-sand veins, 3 = sand xenoliths, 4 = torn and broken sand fragments, 5 = sand intruded by diapir, 6 = undeformed layers.
a, b: Flame-like structures. Well TZ29, depth 5381.30 m; stratigraphical unit O_1q; **c, d:** Complex liquefied diapir. The green dashed line indicates the diapir outline. Well SH2, depth 5573.8 m; stratigraphical unit S_2y.

include upright, symmetrical, undulating, recumbent and overturned folds with rhythmic or intricately convoluted laminations, strongly different vergences and irregular shapes. They result from hydro-plastic deformation, liquefaction and fluidisation by gravity and by 'escaping' pore-water/sediment mixtures due to earthquake-related disturbances (Kuenen, 1958; Lowe, 1975; Guiraud & Plaziat, 1993; Simms, 2003).

At 4303 m in well TZ29, nearly horizontal mud layers are intercalated with laminated siltstones and mudstones of up to 5 cm thick. The orientations of the axial planes of the folds are irregular upright or horizontal (Fig. 5a, 5b). This indicates that convolution occurred by horizontal in-situ compression without slipping (cf. Qiao et al., 2006; Qiao & Li, 2009). The tops of the convolute structures are occasionally eroded away; the abraded structures became subsequently covered by new sediments, thus displaying an abrupt contact with the overlying beds.

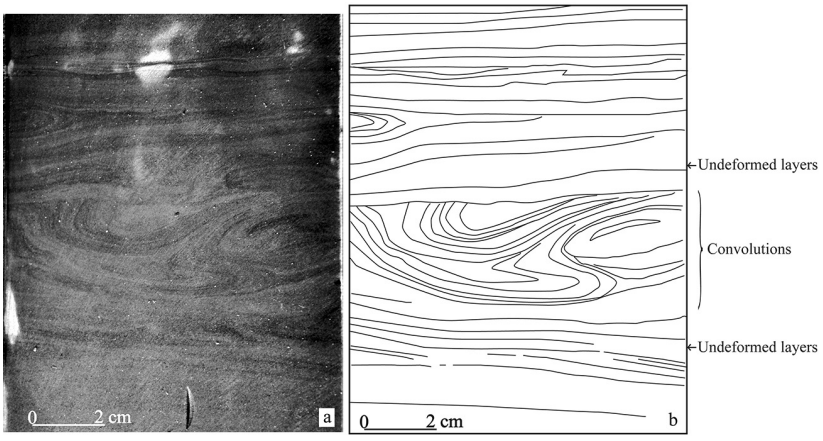

Fig. 5. Hydroplastically formed convolutions between undeformed layers. Well TZ29, depth 4303–4303.12 m; stratigraphical unit O_3q. Note the abrupt contact between the deformed layer and the undeformed overlying layer.

3.5. Dish structures

Dish structures are also formed by hydro-plastic deformation and liquefaction. At a depth of 5567.5 m in well SH2, such deformations occur in thin, laminated brown mudstones and interbedded brown or grey sand layers. The thin sand veins resulted from liquefaction and intruding upwards, broke up into fragments of the thin mud beds and in upwards bending of both ends, thus forming the dish-like structures. Figure 6 shows 'dishes' of mostly 1–1.5 cm wide with a maximum of 3 cm. The thickness of the dish structures is 8 cm. Dish structures are commonly interpreted as triggered by earthquakes (Lowe & LoPiccolo, 1974; Guiraud & Plaziat, 1993; Montenat et al., 2007; Qiao et al., 2011).

3.6. Mixed-layer structures

The term 'mixed-layer structures' refers to gradual upward transitional deformation structures between undeformed beds; the origin is related to the activity of syn-sedimentary faults triggering moderate- to high-magnitude seismic shocks. The structures reflect deformation migrating downwards and passing underlying thin-laminated beds while persistent deformation occurs by a single seismic event (Qiao et. al 1994; Marco & Agnon, 1995; Rodríguez-Pascua et al., 2000). The structures contain four units (Fig. 7), from bottom to top: undeformed laminated layers (Fig. 7b, 1), folded laminated layers (Fig. 7b, 2) also called liquefied convolutions, fractured and fragmented laminated layers (Fig. 7b, 3), and graded layers (Fig. 7b, 4).

Fig. 6. Dish structures in well SH2 at a depth of 5567.5 m; stratigraphical unit S_2y.

At 4713.8 m in well Z12, mixed-layer structures are about 5 cm thick (Fig. 7a). They are composed of laminated grey horizontal sands interbedded with greyish-green silty sands, and intercalated mud fragments deposited in an intertidal beach environment. During seismic activity, the laminated sand layers at the surface were the first to become convoluted or folded under compressional stress; then the deformation succeeded in a constant way downwards, while shear stress liquefied the sand. Subsequently the deformed layers became covered by new sediments. Figure 7 shows these mixed-layer structures, which lack, however, the graded layers of units 4. Liquefied convoluted and mixed-layer structures are interpreted as the result of an earthquake (Qiao et al., 1994; Marco & Agnon, 1995; Rodríguez-Pascua et al., 2000; Qiao et al., 2006; Zhang et al., 2006; Qiao et al., 2011).

3.7. Boudinage-like SSDS and boudinage-like breccias

Boudinage-like soft-sediment deformation structures (B-SSDS) have for the first time been identified in the study area. They refer to unconsolidated sediments under horizontal shear stress that form boudinage-like structures; these occur in rapidly deposited, thick sediments, and are present between undeformed layers with similar lithological properties.

Multiple cycles of B-SSDS are present in the Upper Ordovician in the Manjiaer Depression; they have large thicknesses and a wide distribution. They consist of thin, light grey, calcareous siltstones interbedded between dark grey calcareous mudstones deposited in mixed siliciclastic/carbonate shelf environment. B-SSDS occur, for instance, in well TZ32 at depths of 4094.5 m (Fig. 8a), 4097.6 m (Fig. 8b), 4507.5 m (Fig. 8c) and 4508 m (Fig. 8d). The calcareous sand beds with comparatively higher cohesive muds were sheared and cut off, to form lenticular sand bodies under tensional shear

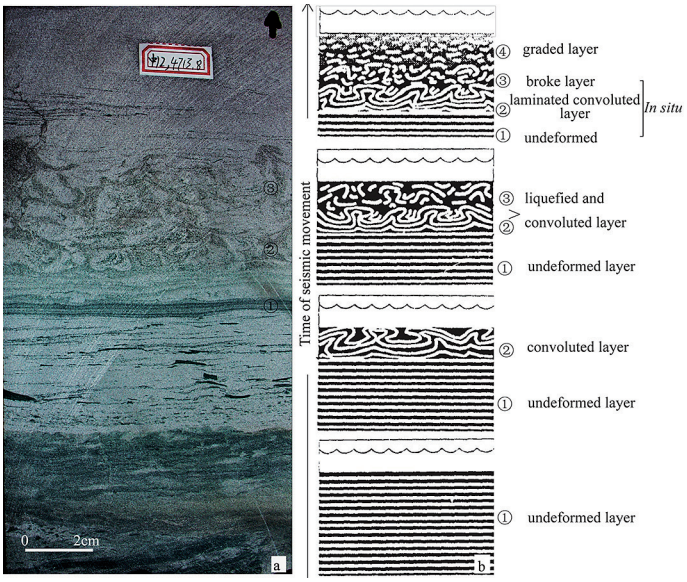

Fig. 7. Mixed-layer structures in well Z12 at a depth of 4713.8 m; stratigraphical unit S_2y. The sketch (b) shows the development of the deformation (modified after Rodríguez-Pascua et al., 2000).

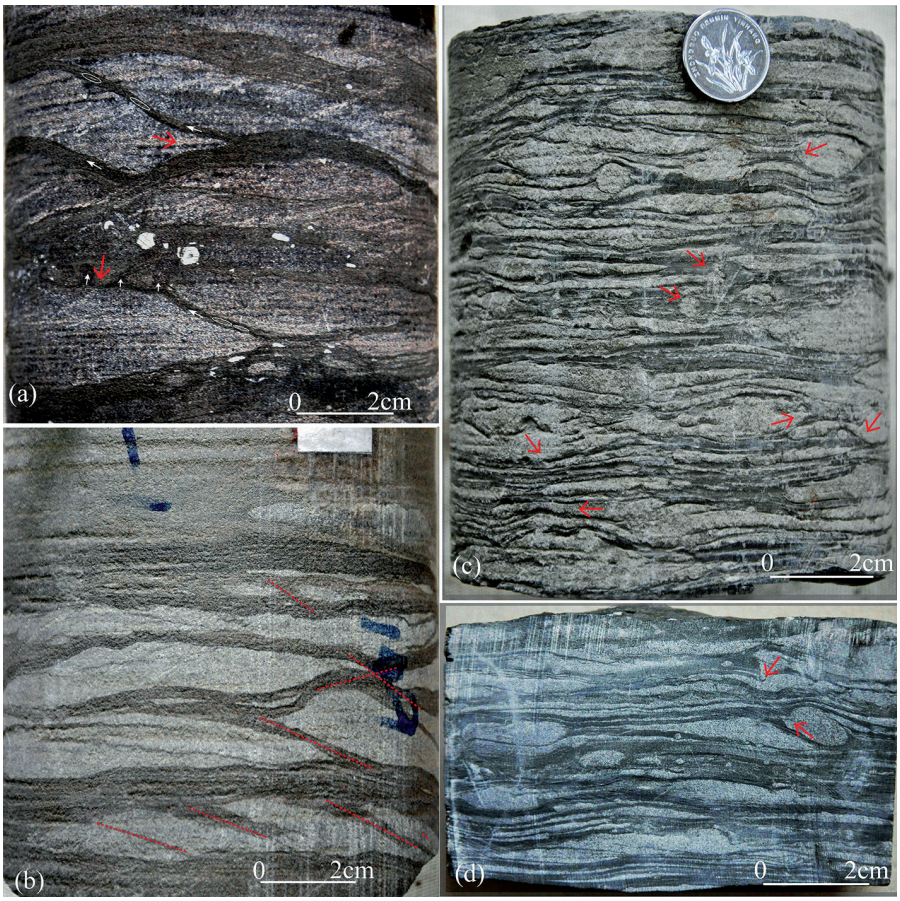

Fig. 8. Boudinage-like soft-sediment deformation structures (B-SSDS) from well TZ32 (Upper Ordovician) in the Manjiaer Depression, Tarim Basin. The red arrows indicate upwards or downwards directed sand veins or bulges formed after liquefaction; the white arrows indicate mud flow and white ellipses contain the captured fragments of sands. **a:** B-SSDS of intruded mudstones which contain some inclusions of sandstones and calcareous fine sandstone. Depth 4094.5 m; stratigraphical unit O_3q; **b:** B-SSDS, and undeformed sediment beds which are in the upper part of cores, consisting of calcareous mudstones (dark grey) with siltstones and fine sandstones (paler units). Depth 4097.6 m; **c:** B-SSDS with extensional shear, small sand veins in or through the B-SSDS; laminated light grey calcareous siltstones alternating with grey silty mudstones. Depth 4507.5 m; **d:** B-SSDS formed under an extensional shear regime. Little sand veins and balls in laminated grey mudstones alternating with light grey calcareous siltstones. Depth 4508.0 m.

stresses. At the same time mud intruded fractures in the sand bodies (see the white arrows in Fig. 8a), dragged along pieces from the bordering zones of the sand bodies, and arranged the fragments according to the flow direction (Fig. 8a, 8b). Some of the sand bodies are still interconnected, whereas other ones were broken with thin and sharp, even curled edges. At 4507.5 m (Fig. 8c), B-SSDS are visible as thin, laminated calcareous sands and dark mud beds of about 1–2 cm thick, sometimes only 0.4 cm. Some sand bodies are alternatingly lenticular and extensional along the bedding. They might easily be misinterpreted as flaser bedding of a tidal-flat setting, but actually they are liquefied-sand veins in lenticular sand bodies (see the red arrows in Fig. 8c, 8d). This suggests that the deformations mainly resulted from tensional shear stresses and behaved hydroplastically and liquefied. The sand bodies behaved differently from the 'flaser' bedding. Sometimes the mud beds were thicker than the sand beds, which tended, under shear tension stress, to break up in one or more groups of shear planes, so that mud could penetrate to form fragments with sharp edges which we call 'boudinage-like breccias' (Fig. 8a, 8b).

3.8. Ball-and-pillow structures, load casts and pseudonodules

Ball-and-pillow structures are present at 5184 m depth in well TZ32; they are mainly composed of regular 'balls' or 'ellipsoids' with diameters between 2 mm and ~1 cm, and they occur scattered in underlying mud beds. Sometimes 2–3 layers of ball-and-pillow structures occur (Fig. 9a). Their deformations, which are comparable with those of loadcasts, resulted from the static pressure of the unconsolidated silt beds that were destroyed while shaking and gravity differentiation took place and sands or silts (the denser material) sank into the underlying (less dense) mud beds to form load-cast structures that evolved into 'ball-and-pillow structures' or pseudonodules (Sims, 1975; Qiao et al., 2006; Van Loon, 2009). Pseudonodules commonly show laminae that follow their more or less circular outside boundary, but some ball-and-pillow structures do not show this (Fig. 9b, 9c). Thus deformed layers alternate with undeformed ones.

4. Deformational setting of the SSDS

4.1. Sequence stratigraphy, seismic sequences and SSDS in the Upper Ordovician

Previous studies of the sequence stratigraphy and palaeogeography indicate that the Upper Ordovician developed in the Tazhong Uplift and the Manjiaer Depression in which the facies changed in the study area from east to west from a mixed shelf to the margin of a carbonate platform (Chen et al., 1999; Liu et al., 2003; Feng et al., 2005; Fan et al., 2007; He et al., 2009, 2010; Zhao et al., 2010). The

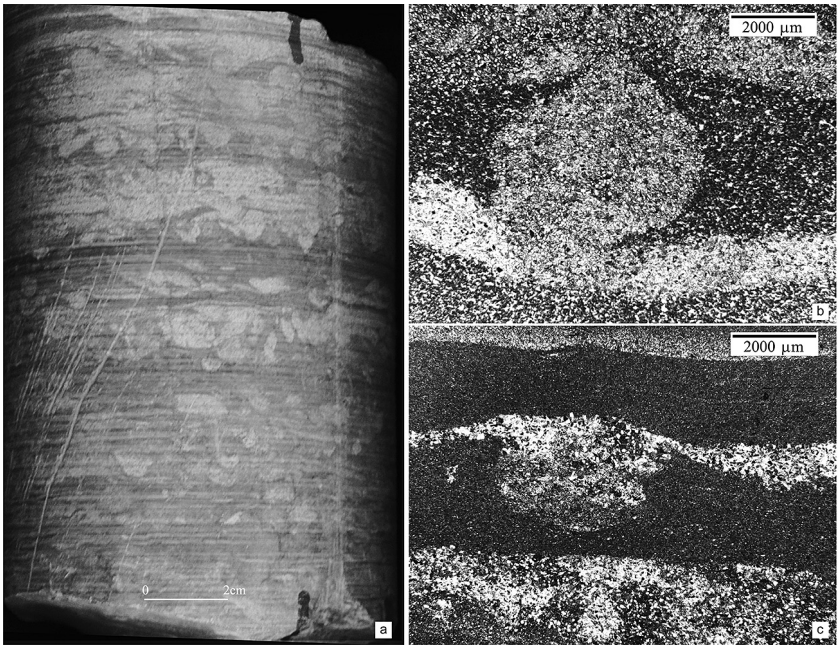

Fig. 9. Ball-and-pillow structures in cores from stratigraphical unit O_3q in well TZ32, Tarim Basin.
a: Calcareous silt balls, interbedded between mudstones, sunk down into mud layers and formed 'layers' of ball-and-pillow structures. Depth 5184 m; **b:** Thin section under plane polarised light showing a 'micro-ball' that sank downwards but was not separated from the parent layer. Depth 5184 m; **c:** Thin section (polarised light) with small-scale load structure. Depth 5184 m.

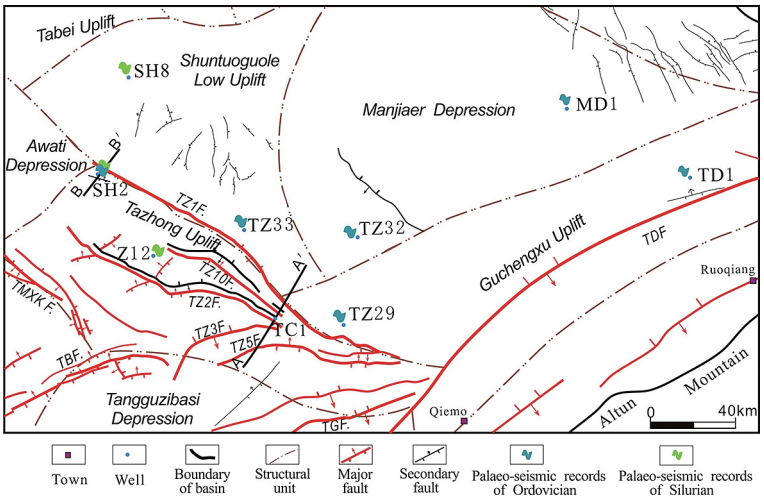

Fig. 10. Fault system and identified seismites in the early Palaeozoic of the central Tarim Basin.
Main faults: TZ1F = Tazhong 1Fault, TZ2F= Tazhong 2 Fault, TZ3F = Tazhong 3 Fault, TZ5F = Tazhong 5 Fault, TZ10F = Tazhong 10 Fault, TBF = Tangbei Fault, TMXKF = Tumuxiuke Fault, TGF = Tanggu Fault, TDF = Tadong Fault.

Upper Ordovician contains 6 stratigraphic sequences: SQ12, SQ13, SQ14, SQ15, SQ16 and SQ17. Based on previous and our own research, we interpret the SSDS described above, considering their types, properties and distribution, as seismites (Figs 10, 11); an important argument is that the layers with SSDS can be correlated in the stratigraphic sequences between the various wells.

SQ13 is the third sequence in the early Late Ordovician, when the rimmed platform margin on

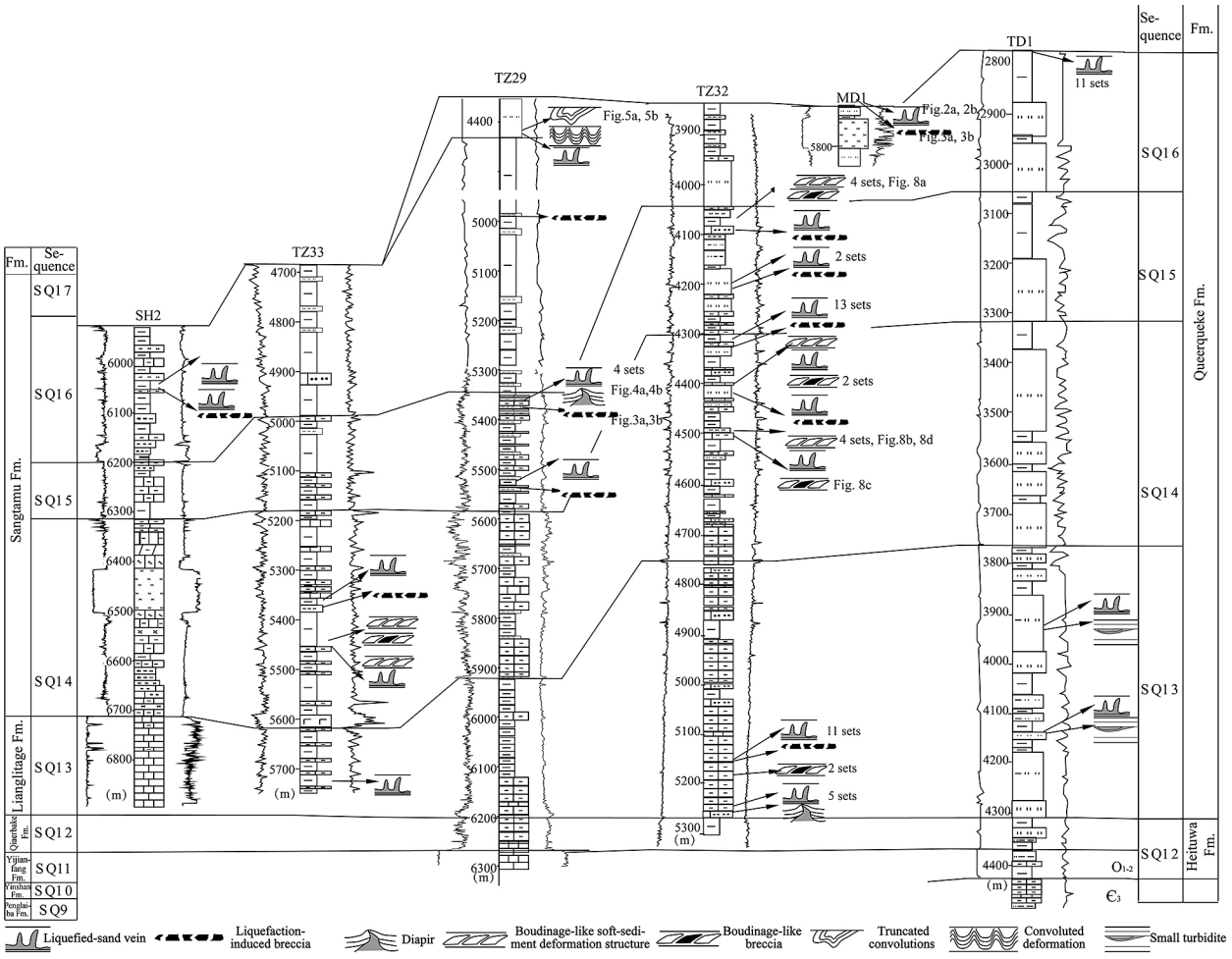

Fig. 11. Correlation of stratigraphical sequences and palaeo-seismic records in the Upper Ordovician in the central part of the Tarim Basin.

the eastern side of the Tazhong Uplift developed (Chen et al., 1999; Fan et al., 2007; He et al., 2009). The seismites in this sequence contain mainly liquefied-sand veins, liquefaction-induced breccias and flames in sediments deposited in a mixed shelf environment (Mount, 1984; He et al., 2010; Zheng et al., 2010). The deformed layers are thin: at a depth of 5742.00~5745.39 m in well TZ33 liquefied-sand veins and liquefaction-induced breccias developed in a layer of about 1–20 cm thick. At a depth of 5273.53~5278.00 m in well TZ32 four sets of sand veins and one set of other SSDS occur in a layer of about 20–40 cm thick. In between these two seismites undeformed dark grey mudstone beds of variable thicknesses occur. At 5172–5188 m in well TZ32, eleven sets of liquefaction-induced breccias are present.

During the formation of SQ14, a transgression took place but there was also volcanic activity. Metre-scale SSDS occur in wells TZ33 and TZ32. At a depth of 5453.00–5461.00 m in well TZ33, five seismites contain predominantly boudinage-like structures and liquefied-sand veins. The individual seismites are 10–70 cm thick with undeformed horizontal siltstones and mudstones in between. This reflects successive events. Most SSDS occur between 4504.21 and 4509.00 m deep in well TZ32. The seismites comprise four sets of liquefied-sand veins and boudinage breccias in 10–20 cm thick layers, with in between a single undeformed layer of 15–40 cm thick.

SQ15 and SQ16 show an ongoing intensive transgression during which B-SSDS, boudinage-like breccias and sand veins developed. The vertical and lateral distribution of SSDS shows that they are more extensive in SQ14 and SQ15 than in SQ13 (Figs 10, 11).

SQ17 is only locally preserved in the central Tarim Basin, due to erosion and non-deposition at the southern and south-eastern margin of regional uplifts (He et al., 2011, 2013). The SSDS in this seismic sequence are different from those in the early Late Ordovician (SQ13-SQ15), and mainly convolutions are found in well TZ29; they formed under compressional conditions.

4.2. Sequence stratigraphy, seismic sequences and SSDS in the Lower-Middle Silurian

At the end of the Ordovician and in the Early Silurian, the southern margin of the Tarim Basin and

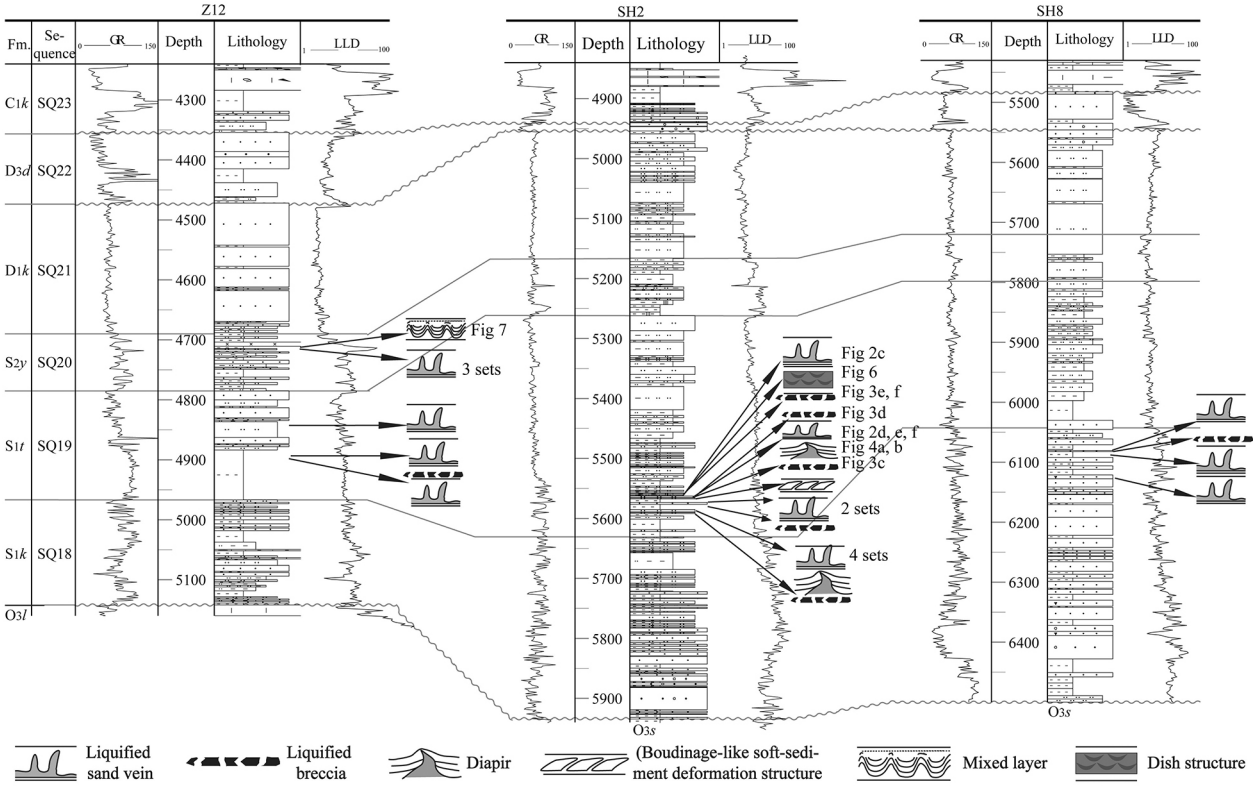

Fig. 12. Correlation of stratigraphic sequences and palaeo-seismic records in the Silurian in the central part of the Tarim Basin.

the southern part of the Manjiaer Depression were uplifted. The succession contains consequently an angular unconformity between the Silurian and the pre-Silurian. The deformation of the northern part of the basin was weak, and a parallel unconformity was formed between the Silurian and the Ordovician. In the Manjiaer-Await Depression, sedimentary facies developed as zones (He et al., 2011, 2013; Lin et al., 2012).

The Silurian developed within the structural framework that had developed at the end of the Ordovician. The depositional environments represented mainly shelf, shore and tidal-flat facies, and a transgression flooded the basin from both the west and the east towards the central part of the basin. The Silurian sediments in the study area accumulated in a shelf to shoreland setting, and can be subdivided into four third-order sequences (SQ18, SQ19, SQ20 and SQ21; Fig. 12) (He et al., 2011; Miao & Fu, 2013).

The cores under study show that SSDS occur mainly in the Lower to Middle Silurian (Figs10, 12). Palaeo-seismic events are recorded in thin Middle Silurian strata of the Tazhong Uplift. SSDS occur in a level of 37 m thick in well SH2, in which 18 layers with SSDS were identified that were most probably triggered by earthquakes, whereas 9 seismic records occur in a 6 m thick level of well Z12, and 9 seismic records occur in an also 6 m thick level of well SH8. The distribution of the SSDS changes not only laterally but also vertically. This reflects a decreasing intensity from early to late phases (not only are SSDS more frequent in SQ19 than in SQ18, but also the intensity of the deformational activity was stronger). The records of seismic activity are concentrated in the south-eastern part of the Tazhong Uplift, increasing in an upward direction (into SQ20).

5. Faults triggering the earthquakes

In the middle Ordovician, the Proto-Tethys Ocean was initially subducted in a northward direction (Yang et al., 1996; Pan et al., 1996). The Late Ordovician, northern Kunlun ocean crust was entirely consumed, which resulted in the middle Kunlun terrain that collided with the Tarim Plate (Xu et al., 2007, 2011). Simultaneously, the southern Altun ocean basin closed, which resulted in a collision orogene with the Tarim Plate (Zhang et al., 2005). The Tarim Basin became converted from an area with a tensional to an area with a compressive flexural regime; this happened between the late Early Cambrian and the middle Late Ordovician. The initial E-W tectonic patterns of the basin gradually changed into N-S trends.

Under the shear tensional tectonic setting during the Early Cambrian to Middle Ordovician, the Tazhong 1 fault (TZ1F) developed. It was the largest and most important fault in the central Tarim Basin and the boundary fault between the Tazhong Uplift and the Manjiaer Depression. It was a syndepositional normal fault that remained active until the early Late Ordovician, when it reversed and changed into a thrust fault (Jia et al., 2004; Tang & Jia, 2007; Li et al., 2008; He et al., 2009, 2010); it stopped acting in the Carboniferous (Figs 10, 13a, 13b). The TZ1F has a length of about 260 km (Fig. 10); it shows a reverse S-shape and runs from NW to SE. It dips to south-west in its western part and to the south in its eastern part. Due to heterogeneity of the stress distribution along the fault's strike, it is divided into segments with different characteristics of basement involvement and slip of the cover (Li et al., 2008). The north-western part of TZ1F cuts through the Precambrian and ends in the Upper Ordovician; the fault activity was here earlier and less than in the other parts of the fault; well SH2 is nearby (Fig. 13b). The middle segment of TZ1F cuts through the Precambrian and ends also in the Upper Ordovician. This fault section is steep and characterised by strong activity and shear; well TZ33 is nearby. The south-eastern segment cuts through the Precambrian and ends in the Carboniferous. It had intense activity, also in branches; well TZ29 is nearby. The TZ1F was the main controlling fault of sedimentation, trap formation, and formation of hydrocarbon reservoirs in the Tazhong Uplift and its adjacent eastern area (Jia et al., 2004; He et al., 2005, 2009).

The just-mentioned wells record that seismic events in the Late Ordovician and the Early-Middle Silurian took place near the TZ1F. Activities along this fault and its branches most probably triggered the earthquakes that are responsible for the seismites under study. The tectonic stress and deformation changed from a shear tensional setting in the early Late Ordovician to a compressional setting at the end of the Late Ordovician, in accordance with the setting of the regional tectonic stress. The seismites of the Silurian might be ascribed to activity of the secondary thrust fault, which had an opposite direction than the TZ1F that triggered the Ordovician seismites. The seismic records indicate that the tectonic environment was extensional with shear during deposition of SQ14 and SQ15, followed by a reversed compressional regime.

Obermeier (1996, 1998), Obermeier et al. (2005) and Qiao et al. (2008) investigated the relationship of the epicentres and the magnitudes of earthquakes to find out about the most distal areas where

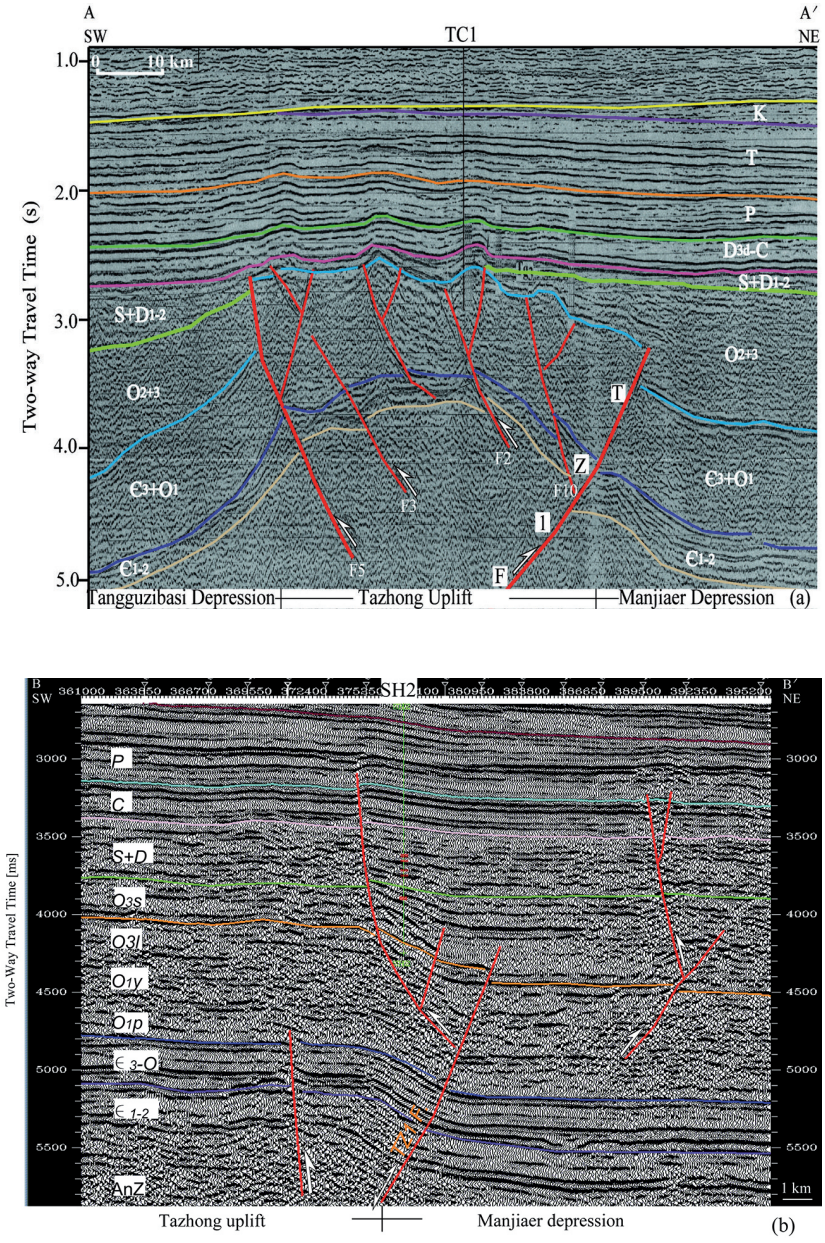

Fig. 13. Interpreted 2-D seismic profiles showing the Tazhong 1 Fault and its associated faults with simultaneously active faults in the Tazhong Uplift and adjacent areas. Faults: TZ1F = Tazhong 1 Fault, F2 = Tazhong 2 Fault, F3 = Tazhong 3 Fault, F5 = Tazhong 5 Fault, F10 = Tazhong 10 Fault. **a:** Profile A-A′ through the southern of the Tazhong Uplift and parts of the Manjiaer Depression. The Tazhong 1 Fault and simultaneously active faults and associated faults are shown; **b:** Profile B-B′ through the northern part of the Tazhong Uplift and parts of the Manjiaer Depression. The Tazhong 1 Fault and its associated fault are shown. The short orange-red bars show the locations of palaeo-earthquake records.

earthquakes could trigger liquefaction, and to clarify the distribution of soft-sediment deformation structures caused by seismic activity. They found that earthquake magnitudes of 9 and 8 *Ms* can cause liquefaction-induced deformations up to 500 and 300 km from the epicentre, respectively. Wells SH2, TZ33 and TZ29, situated at about 1 to 6 km from the TZ1F or its secondary faults, are the closest to these faults; wells Z12, SH8 and TZ32 are the farther away, viz. about 24–47 km from the TZ1F, and the farthest wells are MD1 and TD1, with a distance of about 150–270 km from the TZ1F. These wells are thus located at distances from active faults that make it possible that earthquakes with magnitudes surpassing 8 *Ms* be reflected in all of them. The SSDS in SQ14 of wells TZ33 and TZ32 are observed about 100 km away from the above-mentioned wells (Fig. 12a), and the strata, lithology and style of the SSDS are comparable. During the accumulation of sequences SQ14 to SQ15, an extensional shear regime ruled in the area of the two wells, and the earthquake magnitude near the epicentre may have been 7 *Ms*. The seismites in well Z12 may also have been triggered by activity of the fault TZ10F in the centre of the Tazhong Uplift, which was active simultaneously with or slighter later than TZ1F. The lack of seismically triggered SSDS in wells TD1 and MD1 must be ascribed to the larger distance from TZ1F; there were no other faults near wells TD1 and MD1 active during the Late Ordovician (He et al., 2013).

The seismic records suggest at least 50 strong earthquakes during the time-span of 447–444 Ma (Late Ordovician), and at least 27 times during the time-span of 436–421 Ma (Middle Silurian). Along the Tazhong 1 fault, the intensity and the nature of the tectonic and seismic activities were different. The rising Tazhong Uplift is related with pulsed seismic events. The structure and sedimentation were consequently different along this fault from place to place. The cores under study reveal ongoing seismic activity. More details may be obtained by further study.

6. Significance for hydrocarbon accumulation

The Ordovician and Silurian earthquakes not only induced deformations of unconsolidated sediments but also broke up and deformed the consolidated strata. This resulted in structures that now act as hydrocarbon reservoirs. Main oil and gas reservoirs have been found in the hanging walls and footwalls of the Tazhong 1 fault zone in the centre of the Tarim Basin (He, 1995; Jia et al., 2004; Jin et al., 2005; Gu et al., 2005; He et al., 2009). On the hanging wall of the TZ1F, both the flat reefs at the margin of the carbonate platform and complex, fractured carbonate reservoirs form important hydrocarbon reservoirs in the Upper Ordovician and Lower Ordovician, respectively. The footwalls of the TZ1F did not yield a valuable discovery for a long time because of the lack of structural and stratigraphic traps for hydrocarbon accumulation. A new series of fractured carbonate gas reservoirs have, however, recently been found in the Lower Ordovician and sandstone oil reservoirs were found in the Lower Silurian. Cambrian to Middle Ordovician shales, mudstones and lime-mudstones are here the main hydrocarbon source rocks, and the first large-scale migration of oil and gas took place in the Late Ordovician (Liang et al., 2000; Zhao et al., 2006).

Fracture development during the Late Ordovician was a main controlling factor for hydrocarbon accumulation. The faults that caused the earthquakes that most probably triggered the deformations in the seismites, acted as good migration channels for the oil and gas. Intensive cracks near the active seismic fault may form places where oil and gas is stored. This requires further study.

7. Conclusions

The following four conclusions can be drawn from the present study.

(1) Numerous soft-sediment deformation structures (SSDS) of various types were identified in deep drilling cores of the Upper Ordovician and Lower to Middle Silurian in the centre of the Tarim Basin. They occur in sediments accumulated in shelf, shore and tidal–flat environments. The deformation was triggered by earthquakes. The Tazhong 1 Fault (TZ1F) and its reserved-direction secondary faults were the main seismogenic fault.

(2) The distribution, properties and morphology of the seismically induced SSDS were controlled by the regional tectonic regime; this provides insight into the nature, time, pulses, frequency and locations of the tectonic activity during the main tectonic movements, which are rare proofs of tectonic events with pulsed and cyclic events. They also indicate that the Tazhong 1 fault acted periodically and in several cycles, controlling the uplift of the Tazhong area. The tectonic regime changed from tensional shear to compressional during the early Late Ordovician to middle Silurian. The intensities of the tectonic movements enhanced along the TZ1F both with time and from west to east.

(3) The seismites under study are significant for reconstruction of the tectonic evolution and palaeogeography, and also for insight into the formation and development of fractured reservoirs in consolidated rocks, and of the different time-spans during which flow migration and accumulation took place. The results from the seismite analysis are consequently important for oil and gas exploration.

(4) The seismites under investigation, present in cores from eight wells in the central part of the Tarim Basin, indicate that a more precise understanding of the palaeo-seismic events may be obtained by further study.

Acknowledgements

This study was financially supported by the Science and Technology Project of SINOPEC Co. (No. KY2013-s-024; YPH08110), the Innovation Group of National Natural Science Foundation of China (No. 40921001), the Special Project of Ministry of Land and Resources of China (No. 201011034) and of the Nation (2011ZX05005-002). The China Petroleum & Chemical Corporation (SINOPEC) and China National Petroleum Company (CNPC) supplied the cores of the drilling wells for this research. We are grateful to Professors X.Y. Cai, Z.M. Wang, L.X. Qi, T.Z. Huang, Z.Y. Xiao and L.S. Ye for their support in research. We are also grateful the re-

views by Dr Evert van de Graaf, Dr Tom J.A. Reijers and Prof. A.J. (Tom) Van Loon for helpful and constructive suggestions.

References

Allen, J.R.L., 1982. *Sedimentary structures, their character and physical basis*, Vol. 2. Developments in Sedimentology. Elsevier (Amsterdam) 30B, 663 pp.

Blanc, E.J.P., Blanc-Alétru, M.C. & Mojon, P.O., 1998. Soft-sediment deformation structures interpreted as seismites in the uppermost Aptian to lowermost Albian transgressive deposits of the Chihuahua Basin (Mexico). *Geologische Rundschau* 86, 875–883.

Brodzikowski, K. & Van Loon, A.J., 1987. A systematic classification of glacial and periglacial environments, facies and deposits. *Earth-Science Reviews* 24, 297–381.

Chen, J., Van Loon, A.J., Han, Z. & Chough, S.K., 2009. Funnel-shaped, breccia-filled clastic dykes in the Late Cambrian Chaomidian Formation (Shandong Province, China). *Sedimentary Geology* 221, 1–6.

Chen, J.S., Wang, Z.Y., Dai, Z.Y., Ma, Q., Jiang, Y.Q. & Tan, X.C., 1999. Study of the middle and upper Ordovician rimmed carbonate platform system in the Tazhong area, Tarim Basin. *Journal of Palaeogeography* 1, 8–17 (in Chinese with English abstract).

Du, Y.S., 2011. Discussion about studies of earthquake event deposit in China. *Journal of Palaeogeography* 13, 581–590 (in Chinese with English abstract).

Du, Y. & Han X., 2000. Seismo-deposition and seismites. *Advances in Earth Science* 15, 389–394 (in Chinese with English abstract).

Ettensohn, F.R., Zhang, C., Gao, L., & Lierman, R.T., 2011. Soft-sediment deformation in epicontinental carbonates as evidence of paleoseismicity with evidence for a possible new seismogenic indicator: accordion folds. *Sedimentary Geology* 235, 222–233.

Fan, T.L., Yu, B.S. & Gao, Z.Q., 2007. Characteristics of carbonate sequence stratigraphy and its control on oil-gas in Tarim Basin. *Geoscience* 21, 57–65 (in Chinese with English abstract).

Feng, Z.Z., Bao, Z.D., Wu, M.B., Jin, Z.K. & Shi, X.Z., 2005. *Lithofacies paleogeography of the Cambrian and Ordovician in Tarim area in China*. Beijing Publishing House (Beijing), 186 pp. (in Chinese with English abstract).

Gu, J.Y., Zhang, X.Y., Luo, P., Luo, Z. & Fang, H., 2005. Development characteristics of organic reef-bank complex on Ordovician carbonate platform margin in Tarim Basin. *Oil & Gas Geology* 26, 277–283 (in Chinese with English abstract).

Guiraud, M. & Plaziat, J.C., 1993. Seismites in the fluviatile Bima sandstones: identification of paleoseisms and discussion of their magnitudes in a Cretaceous synsedimentary strike-slip basin (Upper Benue, Nigeria). *Tectonophysics* 225, 493–522.

He, B.Z., Jiao, C.L., Wang, S.L., Deng, G.Z., Wang, G.H. & He, X.P., 2009. Characteristics and exploration prospect of carbonate platform margin of Late Ordovician Lianglitage Formation in Tazhong area, Tarim Basin. *Acta Geologica Sinica* 83, 1039–1046 (in Chinese with English abstract).

He, B.Z., Qiao, X.F., Xu, Z.Q., Jiao, C.L., Cai, Z.H., Zhang, Y.L. & Su, D.C., 2010. The character and significance of paleo-seismic records of the Late Ordovician in Manjiaer Depression and its adjacent area, Tarim Basin, Xinjiang. *Acta Geologica Sinica* 84, 1805–1816 (in Chinese with English abstract).

He, B.Z., Xu, Z.Q., Jiao, C.L., Li, H.B. & Cai, Z.H., 2011. Tectonic unconformities and their forming: implication for hydrocarbon accumulations in Tarim Basin. *Acta Petrologica Sinica* 27, 253–265 (in Chinese with English abstract).

He, B.Z., Jiao, C.L., Xu, Z.Q., Liu, S.L., Cai, Z.H., Li, H.B. & Zhang, M., 2013. Unconformity structural architecture and tectonic paleo-geography environment: a case of the Middle Caledonian on the northern margin of Tibet Plateau and Tarim Basin. *Acta Petrologica Sinica* 29, 2184–2198 (in Chinese with English abstract).

He, D.F., 1995. Unconformities and oil and gas accumulation in Tarim Basin. *Acta Petrolei Sinica* 16(3): 14–21 (in Chinese with English abstract).

He, D.F., Jia, C.Z., Li, D.S., Zhang, C.J., Meng, Q.R. & Shi, X., 2005. Formation and evolution of polycyclic superimposed Tarim Basin. *Oil & Gas Geology* 26, 64–77 (in Chinese with English abstract).

Jia, C.Z., Sun, D.L. & Zhou, Y.X., 2004. *Paleozoic plate tectonic and continental dynamics of Tarim*. Petroleum Industry Press (Beijing), 202 pp. (in Chinese with English abstract).

Jia, C.Z., Wei, G.Q. & Yao, H.J., 1995. *Oil and gas exploration books in Tarim Basin – tectonic evolution and regional structural geology*. Petroleum Industry Press (Beijing), 70 pp. (in Chinese with English abstract).

Jin, Z.J., Zhang, Y.W. & Chen, S.P., 2005. The process of fluctuations in structure and deposition, Tarim Basin. *Science in China Series D – Earth Science*s 35, 530–539 (in Chinese).

Kuenen, Ph.H., 1958. Experiments in geology. *Transactions, Geological Society Glasgow* 23, 1–28.

Li, D.H., Liang, D.G., Jia, C.Z., Wang, G., Wu, Q.Z. & He, D.F., 1996. Hydrocarbon accumulation in Tarim Basin, China. *American Association of Petroleum Geologists Bulletin* 80, 1587–1603.

Li, Y.J., Wu, G.Y., Meng, Q.L., Yang, H.J., Han, J.F., Li, X.S. & Dong, L.S., 2008. Fault systems in central area of the Tarim Basin: geometry, kinematics and dynamic settings. *Chinese Journal of Geology* 43, 82–118 (in Chinese with English abstract).

Liang, D.G., Zhang, S.C., Zhang, B.M. & Wang, F.Y., 2000. Understanding on marine oil generation in China based on Tarim Basin. *Earth Science Frontiers* 7, 534–547 (in Chinese with English abstract).

Lin, C.S., Li, S.T., Liu, J.Y., Qian, Y.X., Luo, H., Chen, J.Q., Peng, L. & Rui, Z.F., 2011. Tectonic framework and paleogeographic evolution of the Tarim basin during the Paleozoic major evolutionary stages. *Acta Petrologica Sinica* 27, 210–218 (in Chinese with English abstract).

Lin, C.S., Yang, H.J., Liu, J.Y., Rui, Z.F., Cai, Z.Z., Li, S.T. & Yu, B.S., 2012. Sequence architecture and deposi-

tional evolution of the Ordovician carbonate platform margins in the Tarim Basin and its response to tectonism and sea-level change. *Basin Research* 24, 559–582.

Liu, Z.B., Yu, B.S., Chen, X.L., Gao, Z.Q., Chao, Q.G., Li, T.Y. & Yu, Z.B., 2003. Sequence stratigraphy and sedimentary characters of submarine fan of middle-upper Ordovician, in Tadong area, the Tarim basin. *Geoscience – Journal of Graduate School, China University of Geosciences* 17, 408–414 (in Chinese with English abstract).

Lowe, D.R., 1975. Water escape structures in coarse-grained sediments. *Sedimentology* 22, 157–204.

Lowe, D.R. & LoPiccolo, R.D., 1974. The characteristics and origins of dish and pillar structures. *Journal of Sedimentary Petrology* 44, 484–501.

Maltman, A., 1984. On the term 'soft-sediment deformation'. *Journal of Structural Geology* 6, 589–592.

Maltman, A.J., 1987. Shear zones in argillaceous sediments – an experimental study. [In:] M.E. Jones & R.M.F. Preston (Eds): *Deformation of sediments and sedimentary rocks*. Geological Society, London, Special Publications, 29 pp.

Maltman, A. (Ed.), 1994. *The geological deformation of sediments*. Chapman & Hall (London), 362 pp.

Marco, S. & Agnon, A., 1995. Prehistoric earthquake deformations near Masada, Dead Sea graben. *Geology* 23, 695–698.

McCalpin, J. (Ed.), 1996. *Paleoseismology.* Academic Press (New York), 382 pp.

Miao, Q. & Fu, H., 2013. Sequence stratigraphy of the Silurian strata in the northern and central Tarim Basin. *Sedimentary Geology and Tethyan Geology* 33, 34–41 (in Chinese with English abstract).

Mills, P.C., 1983. Genesis and diagnostic value of soft-sediment deformation structures – a review. *Sedimentary Geology* 35, 83–104.

Montenat, C., Barrier, P., d'Estevou, P.O. & Hibsch, C., 2007. Seismites: an attempt at critical analysis and classification. *Sedimentary Geology* 196, 5–30.

Moretti, M., Alfaro, P., Caselles, O. & Canas, J.A., 1999. Modelling seismites with a digital shaking table. *Tectonophysics* 304, 369–383.

Moretti, M. & Van Loon, A.J., 2014. Restrictions to the application of 'diagnostic' criteria for recognizing ancient seismites. *Journal of Palaeogeography* 3 (162–173).

Mount, J.F., 1984. Mixing of siliciclastic and carbonate sediments in shallow shelf environments. *Geology* 12, 432–435.

Nichols, R.J., Sparks, R.S.J. & Wilson, C.J.N., 1994. Experimental studies of the fluidization of layered sediments and the formation of fluid escape structures. *Sedimentology* 41, 233–253.

Obermeier, S.F., 1996. Use of liquefaction-induced features for paleoseismic analysis – an overview of how seismic liquefaction features can be distinguished from other features and how their regional distribution and properties of source sediment can be used to infer the location and strength of Holocene paleo-earthquakes. *Engineering Geology* 44, 1–76.

Obermeier, S.F., 1998. Liquefaction evidence for strong earthquakes of Holocene and latest Pleistocene ages in the states of Indiana and Illinois, USA. *Engineering Geology* 50, 227–254.

Obermeier, S.F., Olson, S.M. & Green, R.A., 2005. Field occurrences of liquefaction-induced features: a primer for engineering geologic analysis of paleoseismic shaking. *Engineering Geology* 76, 209–234.

Ogg, J.G., Ogg, G. & Gradstein, F.M., 2008. *The concise geological time scale.* Cambridge University Press (London), 77 pp.

Oliveira, C.M.M., Hodgson, D.M. & Flint, S., 2009. Aseismic controls on in situ soft-sediment deformation processes and products in submarine slope deposits of the Karoo Basin, South Africa. *Sedimentology* 56, 1201–1225.

Owen, G., 1987. Deformation processes in unconsolidated sands. [In:] M.E. Jones & R.M.F. Preston (Eds): *Deformation of sediments and sedimentary rocks.* Geological Society, London, Special Publications 29, 11–24.

Owen, G. & Moretti, M., 2011. Identifying triggers for liquefaction-induced soft-sediment deformation in sands. *Sedimentary Geology* 235, 141–147.

Owen, G., Moretti, M. & Alfaro, P., 2011. Recognising triggers for soft-sediment deformation: current understanding and future directions. *Sedimentary Geology* 235, 133–140.

Pan, Y.S., Zhou, W.M., Xu, R.H., Wang, D.A., Zhang, Y.Q. & Xie, Y.W., 1996. Geological characteristics and evolution of the Kunlun Mountains region during the Early Palaeozoic. *Science in China, Series D – Earth Science*s 39, 337–347 (in Chinese).

Perucca, L.P., Godoy, E. & Pantano, A., 2014. Late Pleistocene-Holocene earthquake-induced slumps and soft-sediment deformation structures in the Acequion River valley, Central Precordillera, Argentina. *Geologos* 20, 147–156.

Qiao, X.F., Song, T., Gao, L.Z., Peng, Y., Li, H.B, Gao, L., Song, B. & Zhang, Q.D., 1994. Seismic sequence in carbonate rocks by vibrational liquefaction. *Acta Geologica Sinica* 7, 243–265 (in Chinese with English abstract).

Qiao, X.F., Song, T.R., Gao, L.Z., Li, H.B., Peng, Y., Zhang, C.H., & Zhang, Y.X., 2006. *Seismic records in strata (ancient earthquake)*. Geological Publishing House (Beijing), 263 pp. (in Chinese with English abstract).

Qiao, X.F., Li, H.B., Wang, S.T., Guo, X.P., Si, J.L. & Zong, W.G., 2008. Paleoseismic evidence of the Talas-Ferghana srike-slip fault during early Jurassic, Xinjiang. *Acta Geologica Sinica* 82, 721–730. (in Chinese with English abstract)

Qiao, X.F. & Li, H.B., 2009. Effect of earthquake and ancient-earthquake on sediments. *Journal of Palaeogeography* 11, 593–610. (in Chinese with English abstract)

Qiao, X.F., Guo, X.P., Ye, L.S., He, B.Z. & Zhou, W., 2011. Paleoseismic evidence of the Caledonian Movement at Kartarke Uplift in the Central Tarim, Xinjiang. *Acta Petrologica Sinica* 27, 243–252 (in Chinese with English abstract).

Rodríguez-López, J.P., Meléndez, N., Soria, A.R., Liesa, C.L. & Van Loon, A.J., 2007. Lateral variability of ancient seismites related to differences in sedimentary facies (the syn-rift Escucha Formation, mid-Creta-

ceous, eastern Spain). *Sedimentary Geology* 201, 461–484.

Rodríguez-Pascua, M.A., Calvo, J.P., Vicente, G.D. & Gomez-Gras, D., 2000. Soft-sediment deformation structure interpreted as seismites in lacustrine sediments of the Prebetic Zone, SE Spain, and their potential use as indicators of earthquake magnitude during the Late Miocene. *Sedimentary Geology* 135, 117–135.

Sarkar, S., Choudhuri, A., Banerjee, S., Van Loon, A.J. & Bose, P.K., 2014. Seismic and non-seismic soft-sediment deformation structures in the Proterozoic Bhander Limestone, central India. *Geologos* 20, 89–103.

Seilacher, A., 1969. Fault-grade beds interpreted as seismites. *Sedimentology* 13, 155–159.

Seilacher, A., 1984. Sedimentary structures tentatively attributed to seismic events. *Marine Geology* 55, 1–12.

Simms, M.J., 2003. Uniquely extensive seismites from the latest Triassic of the United Kingdom: evidence for bolide impact? *Geology* 31, 557–560.

Sims, J.D., 1975. Determining earthquake recurrence intervals from deformational structures in young lacustrine sediments. *Tectonophysics* 29, 141–152.

Sims, J.D., 1978. Annotated bibliography of penecontemporaneous deformational structures in sediments. *United States Geological Survey Open File Report* 78–510, 79 pp.

Song T.R. & Liu, Y.X., 2009. Ancient earthquake records and litho-paleogeography. *Acta Sedimentologica Sinica* 27, 872–879 (in Chinese with English abstract).

Tang, L.J. & Jia, C.Z., 2007. *Structure interpretation and stress field analysis in superposition Tarim basin / Series of typical superposition basin hydrocarbon formation and distribution prediction in China*. Science Publishing House (Beijing), 149 pp. (in Chinese with English abstract).

Tian, Z.Y. & Zhang, Q.C., 1997. *Discussion of hydrocarbon-bearing depositional basin of China*. Petroleum Industry Press (Beijing), 275 pp.

Üner, S., 2014. Seismogenic structures in Quaternary lacustrine deposits of Lake Van (eastern Turkey). *Geologos* 20, 79–87.

Valente, A., Ślączka, A. & Cavuoto, G., 2014. Soft-sediment deformation in Miocene deep-sea clastic deposits (Cilento, southern Italy). *Geologos* 20, 67–78.

Van Loon, A.J. & Brodzikowski, K., 1987. Problems and progress in the research on soft- sediment deformations. *Sedimentary Geology* 50, 167–193.

Van Loon, A.J., 2009. Soft-sediment deformation structures in siliciclastic sediments: an overview. *Geologos* 15, 3–55.

Van Loon, A.J., 2014a. The life cycle of seismite research. *Geologos* 20, 61–66.

Van Loon, A.J., 2014b. The Mesoproterozoic 'seismite' at Laiyuan (Hebei Province, E China) re-interpreted. *Geologos* 20, 139–146.

Van Loon, A.J. & Pisarska-Jamroży, M., 2014. Sedimentological evidence of Pleistocene earthquakes in NW Poland induced by glacio-isostatic rebound. *Sedimentary Geology* 300, 1–10.

Waldron, J.W.F. & Gagnon, J.F., 2011. Recognizing soft-sediment structures in deformed rocks of orogens. *Journal of Structural Geology* 33, 271–279.

Wei, C.G., Zhang, S.Q., Jiang, Z.X. & Zhu, J.Q., 2007. Character and significance of Silurian seismite in the Tarim Basin. *Acta Geologica Sinica* 81, 828–833 (in Chinese with English abstract).

Xu, X.S., Wang, Z.J, Wan, F. & Fu, H., 2005. Tectonic paleogeographic evolution and source rocks of the Early Paleozoic in the Tarim Basin. *Earth Science Frontiers* 12, 49–57 (in Chinese with English abstract).

Xu, Z.Q., Yang, J.S., Li, H.B., Zhang, J.X. & Wu, C.L., 2007. *Orogenic plateau: terrain amalgamation, collision and uplift in the Qinghai-Tibet plateau*. Geological Publishing House (Beijing), 458 pp. (in Chinese with English abstract).

Xu, Z.Q., Li, S.T., Zhang, J.X., Yang, J.S., He, B.Z., Li, H.B., Ling, C.S. & Cai, Z.H., 2011. Paleo-Asian and Tethyan tectonic systems with docking the Tarim block. *Acta Petrologica Sinica* 27, 1–22 (in Chinese with English abstract).

Yang, J.S., Robison, P.T., Jiang, C.F. & Xu, Z.Q., 1996. Ophiolites of the Kunlun Mountains, China and their tectonic implications. *Tectonophysics* 258, 215–231.

Zhang, C.H., Liu, D.B., Zhang, C.L. & Wang, Z.Q., 2006. Early Permian seismically induced soft-sediment deformation structure in Bogda region, Xinjiang: stratigraphy records of earthquake in the retroarc collisional foreland basin. *Earth Science Frontiers* 13, 255–266 (in Chinese with English abstract).

Zhang, J.X., Mattinson, C.G., Meng, F.C. & Yu, S.Y., 2005. An Early Palaeozoic HP/HT granulite-garnet peridotite association in the south Altyn Tagh, NW China: P-T history and U-Pb geochronology. *Journal of Metamorphic Geology* 23, 491–510.

Zhao, Z.J., Jia, C.Z., Zhou, X.Y. & Wang, Z.M., 2006. Key factors of oil-gas reservoir-forming and exploration targets in Ordovician in Tazhong area, Tarim Basin. *China Petroleum Exploration* 11(4): 6–15 (in Chinese with English abstract).

Zhao, Z.J., Pan, M., Yang, H.J., Yu, G. & Xu, Y.J., 2010. The source rock of turbidites of Middle Upper Ordovician in Tarim Basin and its tectonic significance. *Geology Science* 45, 681–697 (in Chinese with English abstract).

Zhao, Z.X., Pan, W.Q. & Xiao, J.N., 2000. *Palaeozoic strata and conodonts in Xinjiang*. Petroleum Industry Press (Beijing), 340 pp. (in Chinese)

Zheng, R.C., Zhou, G., Hu, Z.G & Dong, X., 2010. The characteristics of hybrid facies and hybrid sequence of Xiejiawan Member of Ganxi Formation in the Longmenshan area. *Acta Sedimentologica Sinica* 28, 33–41 (in Chinese with English abstract).

Manuscript received 20 January 2014
Revision accepted 13 February 2014